A 2.5D Electrode System Constructed of Magnetic Sb–SnO$_2$ Particles and a PbO$_2$ Electrode and Its Electrocatalysis Application on Acid Red G Degradation

Mengmeng Yuan [1], Nasir Muhammad Salman [1,2] , Hua Guo [1], Zhicheng Xu [1], Hao Xu [1,*], Wei Yan [1], Zhengwei Liao [3] and Yu Wang [3]

[1] Department of Environmental Science and Engineering, Xi'an Jiaotong University, Xi'an 710049, China; yuan1728144281@126.com (M.Y.); salmannasir@uaf.edu.pk (N.M.S.); shohoku777@stu.xjtu.edu.cn (H.G.); Kylezcxu@foxmail.com (Z.X.); yanwei@xjtu.edu.cn (W.Y.)

[2] Department of Structures and Environmental Engineering, University of Agriculture, Faisalabad 38040, Pakistan

[3] Water Affair Science and Technology Research Institute, Shaanxi Water Affair Group, Xi'an 710021, China; water_affairs@163.com (Z.L.); swagwangyu@163.com (Y.W.)

* Correspondence: xuhao@xjtu.edu.cn

Abstract: A novel electrode consisting of a Ti/PbO$_2$ shell and Fe$_3$O$_4$/Sb–SnO$_2$ particles was developed for electrochemical oxidation treatment of wastewater. Scanning electron microscope (SEM), X-ray diffraction (XRD), the current limiting method, toxicity experiments, and high-performance liquid chromatography were adopted to characterize its morphology, crystal structure, electrochemical properties, the toxicity of the wastewater, and hydroxyl radicals. Acid Red G (ARG), a typical azo dye, was additionally used to test the oxidation ability of the electrode. Results indicated that the 2.5D electrode could significantly improve the mass transfer coefficient and •OH content of the 2D electrode, thereby enhancing the decolorization, degradation, and mineralization effect of ARG, and reducing the toxicity of the wastewater. The experiments revealed that, at higher current density, lower dye concentration and higher temperature, the electrochemical oxidation of ARG favored. Under the condition of 50 mA/cm^2, 25 °C, and 100 ppm, the ARG, Chemical Oxygen Demand (COD) and Total Organic Carbon (TOC) removal efficiency reached 100%, 65.89%, and 52.52%, respectively, and the energy consumption and the current efficiency were 1.06 kWh/g COD, 8.29%, and energy consumption for TOC and mineralization current efficiency were 3.81 kWh/g COD, 9.01%. Besides, the Fe$_3$O$_4$/Sb–SnO$_2$ particles after electrolysis for 50 h still had remarkable stability. These results indicated that the ARG solution could be adequately removed on the 2.5D electrode, providing an effective method for wastewater treatment.

Keywords: 2.5D electrode; electrochemical oxidation; the mass transfer coefficient; hydroxyl radicals

1. Introduction

Electrochemical oxidation (EO) is an environmentally friendly technology for treatment of hazardous or refractory contaminants from wastewater [1–5]. The application of EO is highly promising for yielding some useful by-products. Electrodes, especially the anode, are the core of the electrochemical system, therefore, numerous studies have been carried out on the various electrode materials [6–8]. The most common electrocatalytic anodes include titanium-based electrode (Dimension stable anode (DSA electrode), including PbO$_2$ [9,10], Sb–SnO$_2$ [11,12], IrO$_2$ [13] and

RuO_2 [14] electrodes), noble metal electrode and graphite electrode (including common graphite electrode and boron doped diamond electrode [15,16]). Each electrode has some specific properties on account of its advantages and disadvantages [1]. Compared with other electrodes, the DSA electrodes are inexpensive, easy to prepare, and have high catalytic properties and strong stability [1,11,17,18].

The mass transfer process, as a significant restriction of the electrochemical oxidation, is primarily influenced by the electrochemical reactor structure [2]. The EO system has been conducted by using a conventional 2D electrode or by a newly developed 3D cell while both have their limitations regarding practical applications [19]. The traditional 2D electrochemical reactor, including cathodes and anodes, has the mass transfer limitation and the low area–volume ratio [20–22]. On the other hand, 3D electrochemical reactor promotes the mass transfer efficiency, current efficiency, and decreases the energy consumption, whereas relatively low cyclic stability is still an issue [23–25].

During the process of pollutants oxidization in the 2D reactor, the DSA electrode became inactive due to corrosion and the coatings dispersed in solution that also cannot be recycled, which result in serious material waste [26]. In our previous work [27,28], a new electrolytic cell type named 2.5D electrode system was proposed, as shown in Scheme 1. It consists of a DSA anode as the central electrode, and metal oxide coated magnetic particles as the auxiliary electrodes while the use of a magnet conduces to tightly join the central electrode and the auxiliary electrodes as well as to effectively recycle the magnetic particles. In contrast to the 3D reactor, the particles do not scatter in the solution but comes on the surface of the electrode, which increases the real surface area of the electrode and decreases the applied current density on the central electrode, leading to higher current efficiency and stronger electrode stability.
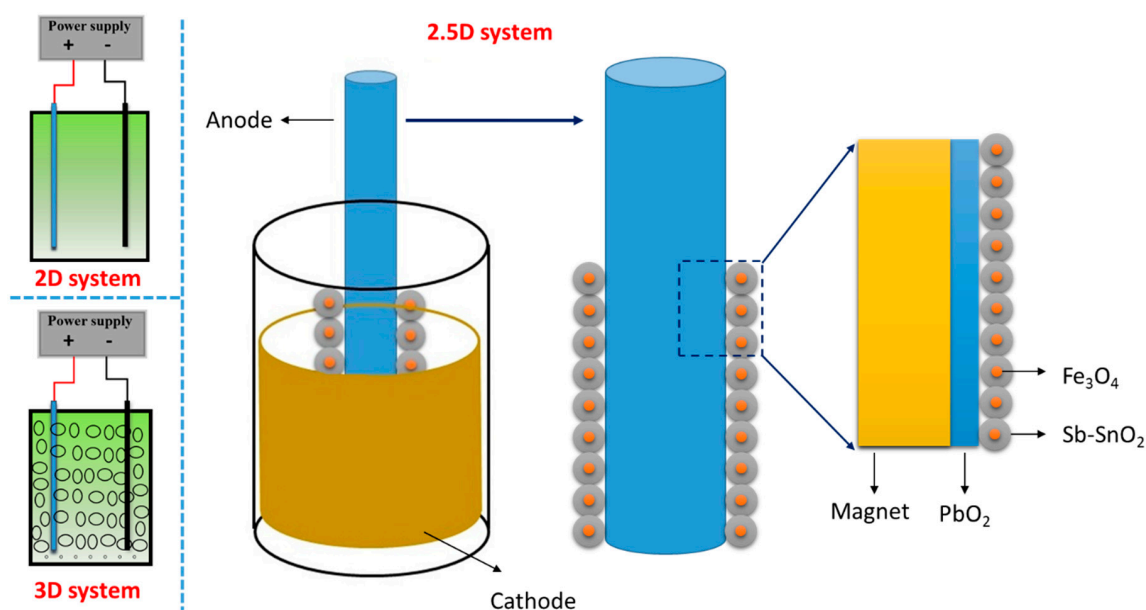
Scheme 1. The structure of 2D, 2.5D, and 3D electrode system.

In the preliminary work, Sb–SnO_2 electrode shell (central electrode) and Fe_3O_4/Sb–SnO_2 magnetic particles (auxiliary electrodes) were used for electrochemical oxidation. The Sb–SnO_2 electrode did not perform well in terms of stability [4], and the accelerated life of the previous 2.5D electrode was only 24 h [27], which would limit its further industrial application. The PbO_2 electrode was a typical titanium-based electrode with excellent stability and high hydroxyl radical yield [29]. However, the leakage of lead ions was an obstacle in further use [7,26]. In this work, the new 2.5D electrode system (as shown in Scheme 1) consists of PbO_2 electrode and Sb–SnO_2 particles. That combination makes full use of the high stability of PbO_2 electrode and the high catalytic activity of Sb–SnO_2 particles. At the same time, it is also expected to reduce the release of lead ions on the surface of PbO_2 electrode by

covering with Sb–SnO$_2$ particles. In this paper, the mass transfer and electrochemical performance of this new 2.5D electrode system were investigated in detail, and the electrocatalytic degradation experiments of relevant target organics were also conducted.

2. Materials and Experiment

2.1. Chemicals and Reagents

All chemicals used in the experiment were obtained from Sinopharm Chemical Reagent Xi'an Co., Ltd. (Xi'an, China), and were of analytical grade without further purification. The pure water fabricated in a water purification system (EPED-S2-D, EPED, Nanjing, China).

2.2. Electrode and Magnetic Powder Preparation

Ti cylinder tube (Purity > 99.6%, BaoTi Ltd., Baoji, China) with a dimension of φ 3 cm × 12 cm were used as the electrode substrate. The Sb–SnO$_2$ layer was coated on the Ti tubes through a brush coating method as reported by our previous work [30,31]. After that, one end of the Ti tubes was sealed with epoxy ethyl ester and polyamide ethyl ester. Finally, the PbO$_2$ coating was fabricated by electrodeposition with an inner layer (α-PbO$_2$) and an outer layer (β-PbO$_2$). The electrodeposition process was conducted in a two-electrode system undercurrent of 10 mA·cm^{-2}. The α-PbO$_2$ and β-PbO$_2$ layers were prepared by electrodeposition at 40 °C for 30 min and 65 °C for 120 min respectively. Details for the electrodeposition process of PbO$_2$ coating can be found in our previous work [6,7,32,33].

The specific preparation method of the Sb–SnO$_2$ magnetic particles was the same as our previous work [27], mainly including heating and stirring, calcination, grinding, and sieving.

The 2D electrode system consisted of titanium tube-based lead dioxide anode and annular copper cathode. In the 2.5D electrode system, the titanium tube-based lead dioxide electrode was covered by a certain amount of Sb–SnO$_2$, magnetic powder used as the anode. The annular copper cathode in the same size as the 2D electrode system was used as the cathode.

2.3. Material Characterizations

The morphology, microstructure and element content of the prepared magnetic particles were analyzed by scanning electron microscopy (SEM: JSM-6390A, JEOL, Tokyo, Japan) equipped with an EDX (energy-dispersive X-ray spectroscopy) detector. X-ray diffraction (XRD: X'pert PRO MRD, PANalytical, Almelo, Holland, Cu Kα) was adopted to analyze crystal structure, with the scanning angle ranging from 10° to 80°. The magnetic property of the granules was determined by a vibrating sample magnetometer (VSM: 735 VSM Controller, LakeShore, Westerville, OH., USA). The powder sample was sealed in a 3 mm × 1 mm space on the vibrating stick and the mass of each sample was recorded. The range of magnet field intensity was set between −7500 Oe and 7500 Oe.

2.4. Electrode System Characterizations

2.4.1. Determination of Mass Transfer Coefficient

The mass transfer coefficient determined by the most common method reported in the literatures is the current limiting method [34,35]. The volume of the test solution was 500 mL, and it contained 0.2 mol/L K$_3$Fe(CN)$_6$ and 0.1 mol/L K$_4$Fe(CN)$_6$ with 1mol/L Na$_2$SO$_4$ as the supporting electrolyte. Then a three-electrode system was scanned with an Amperometric i-t Curve in an electrochemical workstation (CHI 660D, Chenhua, Shanghai, China). The working electrode was a 2.5D electrode and a 2D electrode, respectively. The reference electrode was a saturated calomel electrode. Raising voltage from 0.4 V to 3.4 V every 0.2 V with a scanning interval of 400 s, the results were made into a U–I curve. The corresponding mass transfer coefficient can be calculated through Equation (1).

$$k = \frac{I_{lim}}{nFAC_B},$$ (1)

where k is the mass transfer coefficient, m/s; I_{lim} is the limiting current, A; n is the electron transfer number; F is the Faraday constant (96,500 C·mol^{-1}); A is the plate area, m^2; C_B is the bulk solution concentration, kmol/m^3.

2.4.2. Cyclic Voltammogram Test

The cyclic voltammogram test was performed at an electrochemical workstation (CHI 660D, Chenhua, Shanghai, China) in a three-electrode cell system. Copper sheets acted as the counter electrode, and Ag/AgCl (sat KCl) served as a reference electrode. The measure of cyclic voltammogram test performed in 0.5 mol·L^{-1} Na$_2$SO$_4$ solutions at the scan rate of 0.05 V·s^{-1} from 0 V to 2 V.

2.4.3. The Determination of •OH

Hydroxyl radicals were measured by an indirect method with DMSO as the capture agent [36,37]. 2.5D and 2D electrode were used to electrolysis a 500 mL-volume solution with 250 mmol/L DMSO for 1 h at 40 mA/cm^2, sampling 2 mL every 15 min. The samples were filtered through a 0.45 μm filter, maintained at 25 °C for a certain time, then 2.5 mL pH 4.0 H$_3$PO$_4$–NaH$_2$PO$_4$ and 0.2 mL six mmol/LDNPH were added and diluted to 5 mL. The mixture was maintained at room temperature for 30 min and analyzed by HPLC (Sykam S500, Sykam, Eresing, Germany). HPLC conditions: λ = 355 nm, injection volume: 20 μL, mobile phase: methanol/water = (60/40, *v/v*). The flow rate of 1.0 mL·min^{-1}. Samples were ultrasonically degassed and filtered with a 0.45 μm PTFE filter.

2.5. Electrochemical Oxidation Process

Acid Red G (C$_{18}$H$_{13}$N$_3$Na$_2$O$_8$S$_2$, Chemical Abstracts Service Number (CAS no.) 3734-67-6) and three other organics (including Salicylic acid (CAS no.69-72-7), Phenol (CAS no.108-95-2), and Aniline (CAS no.62-53-3)) were selected as the target organics in the electrochemical oxidation process. Electrochemical oxidation was conducted in a thermostatic glass cell (ϕ = 5 cm) using the two-electrode configuration, and the electrolyte circulated through a peristaltic pump. The 2.5D and 2D electrode were used as the anode and a copper sheet was employed as the cathode. The volume of the electrolyte solutions was 500 mL. To maintain the conductivity of the solution (27.2 mS/cm), 0.1 mol·L^{-1} Na$_2$SO$_4$ was added to the aqueous solution. The experiments were operated with a magnetic stirrer for 120 min, sampling 5 mL every 30 min. A UV-visible spectrophotometer (UV2600A, Unico, Shanghai, China) was employed to measure the absorbance spectra of Acid Red G (ARG), and the maximum absorption peak of ARG was at 505 nm. The Chemical Oxygen Demand (COD) was measured with a water quality tester (ET99722 Lovibond, Shanghai, China). TOC was analyzed by ET1020A TOC analyzer.

The calculation methods of some indexes, such as ARG removal efficiency (η_{ARG}), COD removal efficiency (η_{COD}), TOC removal efficiency (η_{TOC}), current efficiency (*CE*), energy consumption (*EC$_{COD}$*, kWh/gCOD), mineralization current efficiency (*MCE*) and TOC energy consumption (*EC$_{TOC}$*, kWh/gTOC), are shown in the following equations.

$$\eta_{ARG} = \frac{A_0 - A_t}{A_0} \times 100\%, \tag{2}$$

$$\eta_{COD} = \frac{COD_0 - COD_t}{COD_0} \times 100\%, \tag{3}$$

$$\eta_{TOC} = \frac{TOC_0 - TOC_t}{TOC_0} \times 100\%, \tag{4}$$

$$CE = FV \frac{COD_0 - COD_t}{COD_0} \times 100\%, \tag{5}$$

$$EC_{COD} = \frac{UIt}{V(COD_0 - COD_t)}, \tag{6}$$

$$EC_{TOC} = \frac{50UIt}{3V \times TOC_0 \times \eta_{TOC}}, \qquad (7)$$

$$MCE = \frac{nFV(TOC_0 - TOC_t)}{mIt \times 4.32 \times 10^7} \times 100\%, \qquad (8)$$

where A_0 and A_t are the absorbance value in 505 nm of initial wastewater sample and electrolysis at the given times t, COD_0 and COD_t are the COD of initial wastewater sample and electrolysis at the given times t, $g \cdot m^{-3}$. TOC_0 and TOC_t are the TOC of initial wastewater sample and electrolysis at the given times t, $g \cdot m^{-3}$. I is the current (A); U is the cell voltage (V); V is the volume of the electrolyte (m^3); t is the treatment time (min); n is the number of electrons consumed during ARG mineralization (98); 4.32×10^7 is the conversion factor (3600 $s \cdot h^{-1} \times$ 12,000 mg); m is the number of carbon atoms in the ARG molecule (18).

2.6. Toxicity Evaluation of Degradation Result

The concentration of a metal element in the solution after electrolysis was determined by ICP-OES (ICPE-9000, SHIMADZU, Kyoto, Japan).

Biofluorescence method. According to GB 15441-1995, toxicity experiments were carried out to evaluate the toxicity of samples after electrochemical oxidation. Photobacterium phosphoreum T_3 was purchased from the China Microorganisms Collection Center. Three sets of parallel and one control group were set for each sample to test. In the parallel-group, 867 µL of the test sample was added, and in the control group, 867 µL of pure water was added. After contacting with the sample, the broth was placed on a Modulus™ single-tube multi-purpose detector and counted. Relative luminosity significantly negatively correlated with the concentration of toxic components in the water sample. Therefore, the relative luminosity of the water sample can be measured with a bioluminescence photometer to indicate its toxic luminescence level.

3. Results and Discussion

3.1. The Comparison of 2D and 2.5D Electrode

3.1.1. Mass Transfer Coefficient

Figure 1a shows the ampere-voltage curve of 2.5D electrode system under different magnetic particle dosage. As shown in Figure 1a, one can find that the ampere-voltage curve of the 2.5D electrode at different particle dosage has the current plateau. When the particle dosage increased from 0 to 5 g, the plateau current value increased slowly. When the particle dosage increased to 7.5 g and 10 g, the plateau current value was significantly higher than the data when the particle dosage was 0 g. The mass transfer coefficient can be calculated by combining the current platform value with equation 1, as shown in Figure 1b. The corresponding mass transfer coefficients were 0.00148, 0.00172, 0.00206, 0.00361, and 0.00495 $m \cdot s^{-1}$ when the particle dosage was 0 g, 2.5 g, 5 g, 7.5 g, and 10 g. The data confirmed that the addition of particle dosage could increase the electrochemical system mass transfer coefficient.

3.1.2. Hydroxyl Radicals

Hydroxyl radicals are generated from the oxidation of water, as shown in Equation (9). It is the core of electrocatalytic reaction. Hydroxyl radicals were measured by an indirect method with DMSO as the capture agent. HPLC was used to qualitatively determine the •OH content of 2.5D electrodes with different magnetic particle dosage. The variation of •OH content with electrolysis time is shown in Figure 2. The •OH content grew up improperly with the increase of Sb–SnO$_2$ magnetic particle dosage and the extension of electrolysis time as shown in Figure 2. It meant that the •OH yield of the 2.5D electrode system was more than that of the traditional 2D electrode system. When the magnetic

particle was 10 g, the •OH yield of the 2.5D electrode system was the highest. At 60min, the •OH yield of 2.5D electrode system was 673.4 μmol·L^{-1}, while that of 2 D electrode system was 425.8 μmol·L^{-1}.
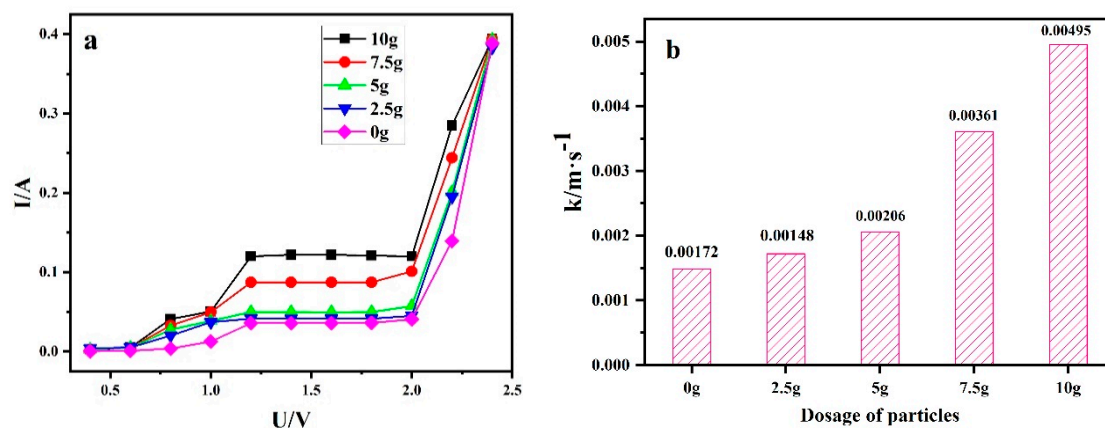
$$H_2O \rightarrow \bullet OH + H^+ + e \tag{9}$$

Figure 1. (**a**) Ampere–voltage of different particle dosage (**b**) the corresponding mass transfer coefficient.
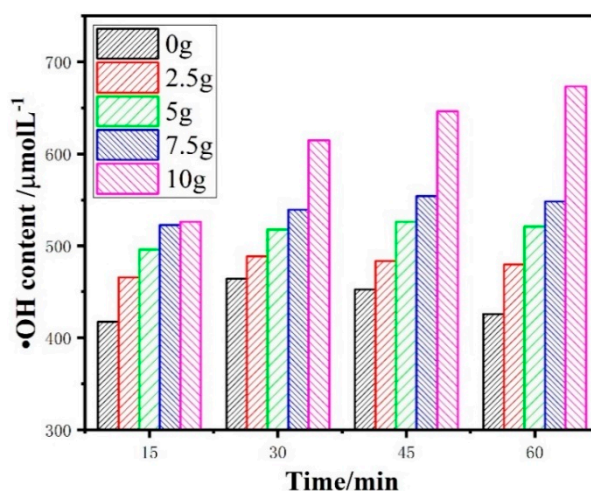

Figure 2. The •OH content under different Sb–SnO$_2$ magnetic particle dosage.

3.1.3. Electrochemically Active Site

Literature reports that the number of electroactive sites on the electrode surface is proportional to the area of its cyclic voltammetry curve. Figure 3 is the cyclic voltammetry curve of a 2.5D electrode system under different Sb–SnO$_2$ magnetic particle dosage. It can be seen from Figure 3 that the introduction of magnetic particles significantly increased the cyclic voltammogram area of the electrode system. This indicates that the number of electrode surface active sites in 2.5D electrode system was larger than that in the traditional 2D electrode system.

Comprehensive appeal results show that the 2.5D electrode system is superior to the traditional 2D electrode system in terms of mass transfer coefficient, hydroxyl radical yield, and surface-active sites. The reason for that phenomenon is that Sb particles are excellent electroactive particles, whose introduction can greatly expand the surface area of lead dioxide electrode. Considering that the electrode surface cannot adsorb more particles magnetically, 10 g was chosen as the number of magnetic particles.
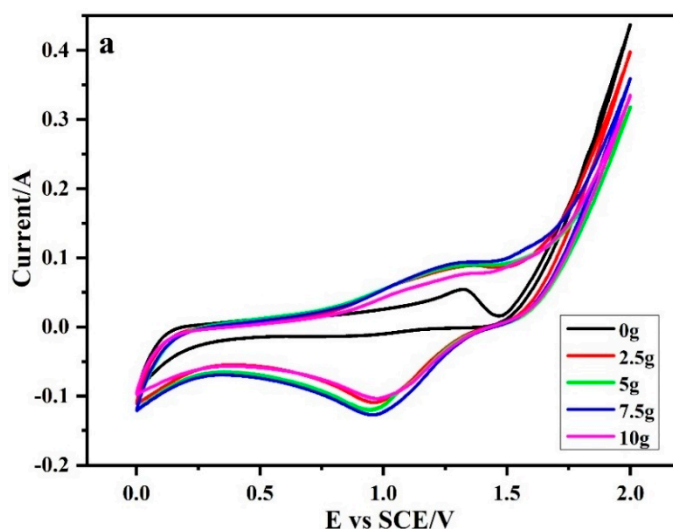
Figure 3. The cyclic voltammetry curve of 2.5D electrode system under different Sb–SnO$_2$ magnetic particle dosage.

3.1.4. Electrocatalytic Capacity Comparison

An electrocatalytic degradation experiment was carried out with ARG as the target. The results are shown in Figure 4 and Table 1. As shown in Figure 4a, the removal efficiency (including η_{ARG}, η_{COD}, and η_{TOC}) of the 2.5D electrode system is higher than that of the 2D electrode system. Meanwhile, the 2.5D electrode system has a higher *CE*, almost twice as much as the 2D electrode, with the current efficiency of 12.21% compared with 7.1%. The EC_{COD} decreases from 1.71 kWh/gCOD to 0.961 kWh/gCOD, as shown in Table 1. From the above results, one can find that the 2.5D electrode system has better performance in the electrocatalytic process than 2D electrode system. It may be because the 2.5D electrode system has a higher mass transfer coefficient, greater hydroxyl radical production, and more surface-active sites than the 2D electrode system.
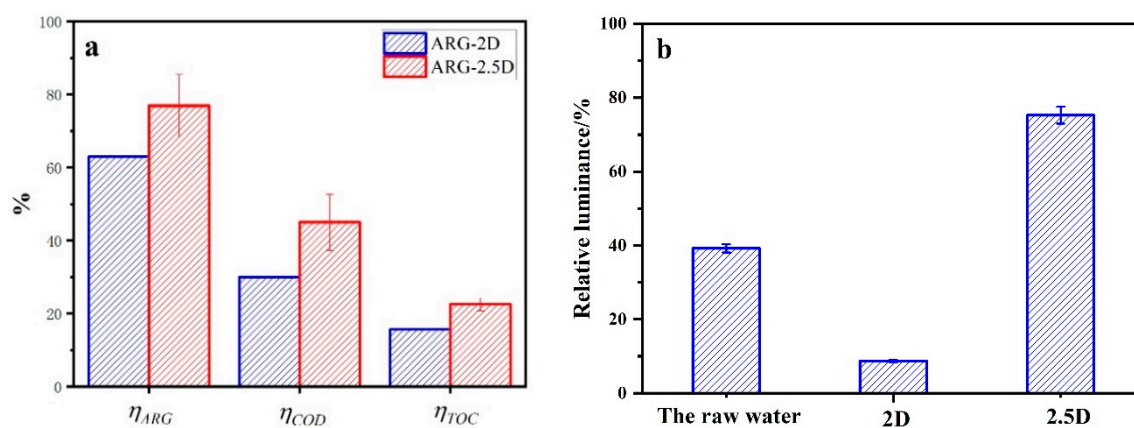

Figure 4. The removal efficiency (**a**) and relative luminance before and after electrolysis (**b**) of Acid Red G (ARG) by 2.5D and 2D electrode (electrolysis condition: ARG 100 ppm, 10 mA/cm^2, 0.1 mol/L Na$_2$SO$_4$, room temperature, and electrolysis time of 1 h).

According to GB/T 15441-1995, the toxicity of wastewater samples before and after degradation by the 2D and 2.5D electrode system were tested, as shown in Figure 4b, indicating that the relative luminosity of samples treated by 2.5D electrode system is higher than that of the raw water. Nevertheless, the relative luminosity of samples treated by the 2D electrode was significantly lower than that of the raw water. It means that the 2.5D electrode system reduced the biotoxicity of the raw water and greatly

increased compared to the 2D electrode system. One of the reasons for this phenomenon is that the electrocatalytic oxidation ability of the 2.5D electrode system is stronger than that of the 2D electrode system. ARG molecules can be decomposed by the 2.5D electrode system to a higher degree and more non-toxic or low-toxic small molecular substances. Another reason is the concentration of lead ions released during electrolysis. The lead dioxide of the 2D electrode system is exposed to the solution. In this case, the lead ion will leak into the solution, increasing the toxicity of the wastewater. Inductively Coupled Plasma (ICP) test results showed that the concentration of a lead ion in the electrolyzed water of 2D electrode system was 0.25 mg/L. For the 2.5D electrode system, the Sb−SnO$_2$ magnetic particles adhere to the lead dioxide electrode surface and can inhibit the leakage of lead ion during the electrolysis. The concentration of lead ion in the electrolyzed water of 2.5D electrode system was 0.10 mg/L, less than that of the 2D electrode system.

Table 1. The parameters comparison of 2.5D and 2D electrode.

		CE/%	EC_{COD}/kWh/gCOD	η_{TOC}/%
ARG [a]	2D	7.10	1.71	15.6
	2.5D	12.2	0.961	22.6
Salicylic acid	2D	5.04	0.45	40.85
	2.5D	7.30	0.32	54.68
Phenol	2D	6.97	0.34	27.04
	2.5D	8.64	0.27	52.77
Aniline	2D	10.05	0.23	28.92
	2.5D	12.06	0.19	56.01

[a] The applied current density was 10 mA/cm^2 for ARG and 50 mA/cm^2 for three other organisms. The electrolysis time was 1 h for ARG and 2 h for three other microorganisms.

To further verify the superiority of the 2.5D electrode system in electrocatalytic capability, three other typical organic compounds (including Salicylic acid, Phenol, and Aniline) were used as degradation targets for electrocatalytic degradation experiments. The results are shown in Figure 5 and Table 1. The η_{COD}-2 h and η_{TOC}-2 h of aniline were 60.18% and 56.01% by using the 2.5D electrode system, which were higher than 35.71% and 28.92% of the 2D electrode system. The *CE* of aniline for the 2.5D electrode system was 12.06%, higher than 10.05% for 2D electrode system. Meanwhile, the EC_{COD} decreased from 0.23 kWh/gCOD to 0.19 kWh/gCOD. Similar results could be obtained when the other two organics were degraded. All the above results show that the 2.5D electrode system has advantages in electrocatalytic capability over the 2D electrode system.

3.2. Degradation of ARG by Using the 2.5D Electrode System

3.2.1. Effect of Current Density

Current density is an important parameter in controlling the reaction rate and has a significant effect on the electrochemical oxidation process. The current density was changed from 10 to 50 mA/cm^2 in the process of degrading the ARG. As shown in Figure 6a,b, current density had a positive effect on the degradation of ARG with the increasing of current density. The η_{ARG} increased from 77.69% to 100% after 120 min of electrolysis. When the current density reached 40 mA/cm^2, the complete discoloration of ARG can be achieved after 60 min. The η_{COD} increased from 52.6% to 65.89% with the raising of current density from 10 to 50 mA/cm^2, but not completely removed. It may be because, of the process of electrochemical oxidation where an azo bond oxidation easily occurred, the intermediate products and other organics continued to be oxidized so that the rate of color removal was higher than the COD reduction. Yao et al. [38] reported that current density was proportional to electrochemical oxidation and could increase •OH production. Therefore, in the 2.5D electrode system, the increasing current density is also beneficial to organic matter removal.
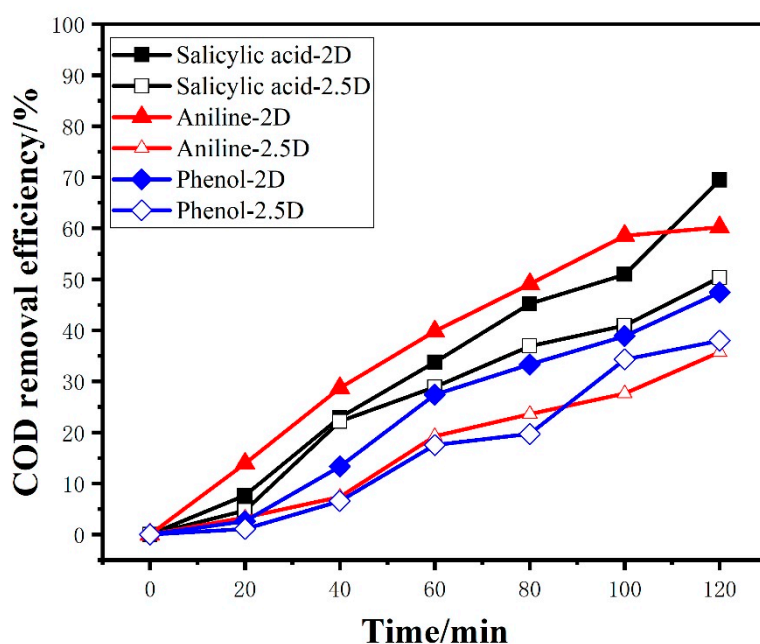
Figure 5. The Chemical Oxygen Demand (COD) removal efficiency of three organic target by 2.5D and 2D electrode (electrolysis condition: concentration 100 ppm, 50 mA/cm², 0.1 mol/L Na₂SO₄, room temperature).
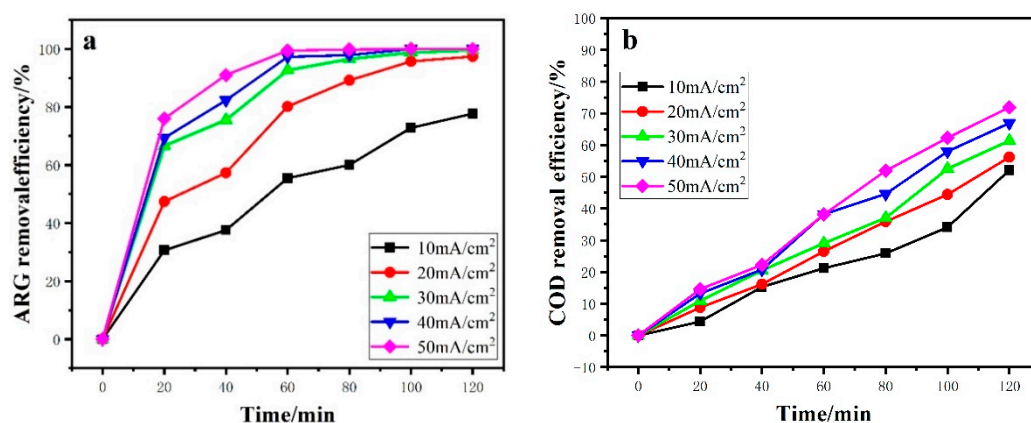

Figure 6. Effect of current density on ARG removal efficiency (**a**) and COD removal efficiency (**b**). Other operating conditions: ARG concentration of 100 ppm and temperature of 25 °C.

From Table 2, it can be seen that with the increase of current density, η_{TOC} increased from 18.64% to 52.51%. However, EC_{COD} and EC_{TOC} both increased, and *CE* and *MCE* gradually decreased. Li et al. [19] considered that with the increase of current density, the reaction of oxygen production increased, which would compete with the degradation of organics, leading to the decrease of current efficiency and the increase of energy consumption.

Table 2. Effect of different factors on ARG degradation by using the 2.5D electrode system.

		CE/%	EC_{COD}/kWh/gCOD	η_{TOC}/%	*MCE*/%	EC_{TOC}/kWh/gTOC
Current density (mA/cm²)	10	5.90	0.22	18.64	3.28	1.43
	20	3.48	0.46	23.76	2.52	2.28
	30	2.56	0.71	27.05	1.90	3.46
	40	2.45	0.83	37.35	1.97	3.74
	50	2.07	1.06	52.51	1.62	4.94

Table 2. *Cont.*

		CE/%	EC_{COD}/kWh/gCOD	η_{TOC}/%	*MCE*/%	EC_{TOC}/kWh/gTOC
Dye concentration (mg/L)	50	0.89	2.43	41.77	0.86	9.13
	100	2.07	1.06	52.52	1.62	4.94
	200	3.08	0.7	35.22	2.55	3.09
	300	3.39	0.66	17.70	1.45	5.60
Temperature (°C)	5	5.76	1.72	40.69	6.8	4.60
	15	6.48	1.46	46.07	7.92	4.03
	25	8.29	1.06	52.52	9.01	3.81
	35	5.79	1.45	62.97	11.11	3.24

3.2.2. Effect of Initial Organic Concentration

Figure 7 shows the effect of initial dye concentration on ARG degradation. As shown in Figure 7a, complete color removal could be achieved when the ARG concentration increased from 50 ppm to 300 ppm. However, it would take more time to achieve the complete decolorization for higher ARG concentration solution. The η_{COD} after 120 min electrolysis was 76.17%, 71.96%, 56.05%, and 48.18% when the initial ARG concentration was 50, 100, 200, and 300 mg·L^{-1}, respectively. Table 2 also shows that EC_{COD} and EC_{TOC} significantly reduced with increasing initial dye concentration, while *CE* and *MCE* significantly increased with the increasing initial dye concentration.
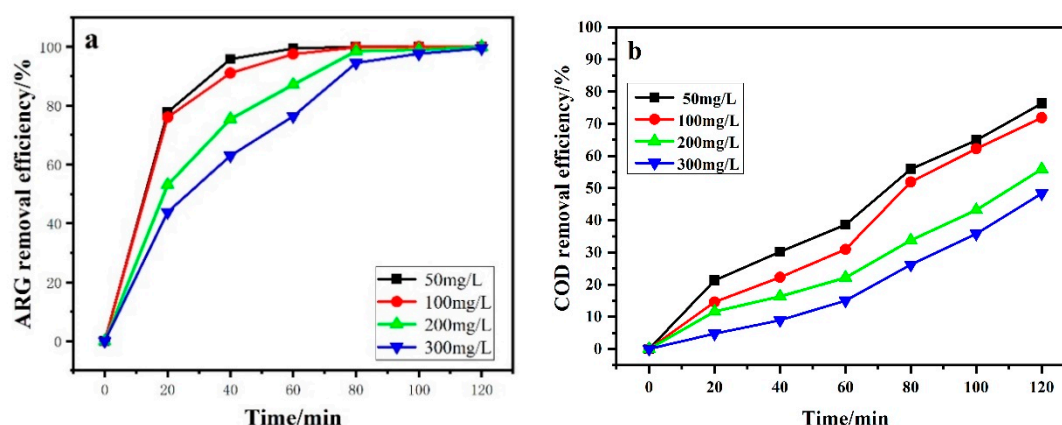

Figure 7. Effect of dye concentration on ARG removal efficiency (**a**) and COD removal efficiency (**b**). Other operating conditions: Current density of 50 mA/cm^2 and temperature of 25 °C.

The electrocatalytic oxidation process is controlled by mass transfer. At low initial ARG concentrations, the electrochemical reaction is faster than the diffusion process. The dye molecule was expected to be degraded completely at the electrode–solution interface. When the initial ARG concentrations increased, the amount of ARG molecule achieved the anode surface was larger than that in the low concentration solution. Thus, more ARG molecules reacted with the •OH on the anode surface in the high concentration solution [2]. The amount of •OH generated on the surface of the PbO$_2$ anode at a given current density fixed. Active free radicals generated on the electrode surface were insufficient for pollutant degradation with increasing ARG concentration. Then the η_{COD} decreased with the increase of the initial ARG concentrations, while EC_{COD} and EC_{TOC} decreased with the increase of the initial ARG concentrations.

3.2.3. Effect of Temperature

Figure 8 shows the effect of temperature on ARG removal efficiency and COD removal efficiency. One can find that when the temperature was lower than 25 °C, η_{ARG} and η_{COD} increased as the temperature rose. However, η_{ARG} and η_{COD} declined when the temperature rose to 35 °C. As shown

in Table 2, η_{TOC} follows the same rules. Generally speaking, when the temperature is higher, the chemical reaction rate increases, thereby increasing the utilization of •OH. When the temperature does not exceed 25 °C, the experimental results prove this. However, when the temperature exceeds 25 °C, all chemical reactions in the electrolytic cell are accelerated, including various side reactions. The oxygen evolution side reaction reduced the utilization rate of hydroxyl radical and current efficiency, and finally reduced the overall reaction effect.
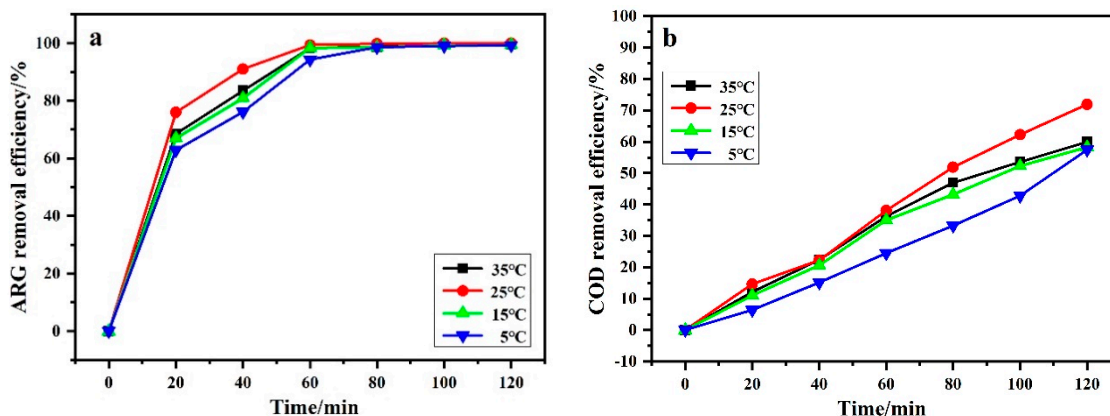

Figure 8. Effect of temperature on ARG removal efficiency (**a**) and COD removal efficiency (**b**). Other operating conditions: Current density of 50 mA/cm^2 and ARG concentration of 100 ppm.

3.3. The Stability of Fe$_3$O$_4$/Sb–SnO$_2$

The XRD patterns, magnetization curves, and surface element content of the magnetic particles before and after 50 h-electrolysis are shown in Figure 9 and Table 3. As shown in Figure 9a, there were the diffraction peaks of Fe$_3$O$_4$ (35.51°), Fe$_2$O$_3$ (33.1°), TiO$_2$ (62.8°), Sb–SnO$_2$ (26.6° and 51.8°), which were consistent with previous researches. After the electrolysis for 50 h, there was no change in particle diffraction peak. It can be seen from Table 3 that, after electrolysis, the element content on the surface of particles changed slightly. Sn and Sb decreased, while Fe and Ti increased. It indicates that the surface of magnetic particles dissolved to a certain extent after electrolysis for 50 h, resulting in increased exposure of ferric oxide. As shown in Figure 9b, the magnetic properties of the particles increased after use. These results indicate that Sb–SnO$_2$ magnetic particles had better stability than Sb–SnO$_2$ electrodes. More importantly, this 2.5D electrode system provides excellent convenience for particle replacement and is conducive to the continuity of the electrocatalytic process improvement.
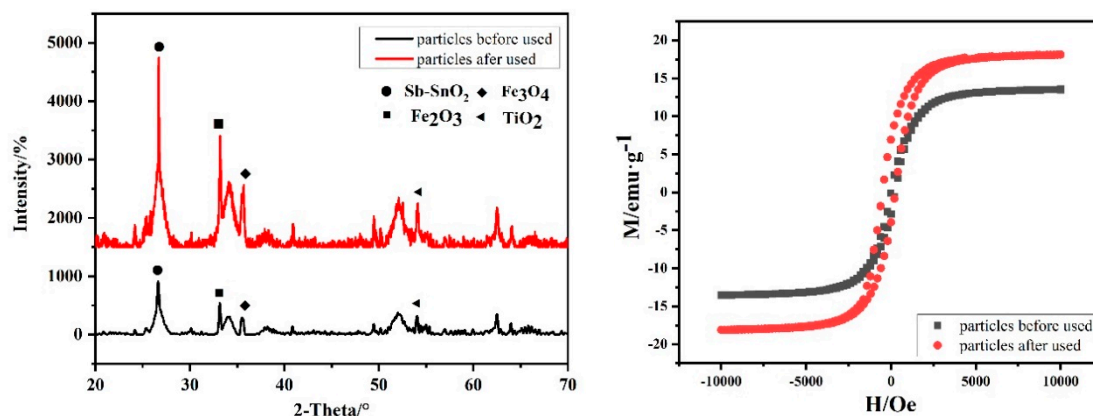

Figure 9. XRD patterns (**a**) and magnetization curves (**b**) of magnetic particles before and after electrolysis.

Table 3. The surface element content of magnetic particles before and after electrolysis.

	Sn	Sb	Fe	Ti	C	O
Before electrolysis	23.57	3.03	7.23	11.89	10.26	44.01
After 50 h electrolysis	20.47	2.86	11.24	12.67	10.38	42.38

4. Conclusions

In this study, the PbO_2 electrode and the Sb–SnO_2 electrode were combined by a magnet to construct a newly assembled 2.5D electrode. Due to the existence of Fe_3O_4/Sb–SnO_2 particles, it proved that the 2.5D electrode could improve the mass transfer coefficient and increase •OH content, relative to the traditional 2D electrode. The degradation experiments showed that the 2.5D electrode could improve the performance of decolorization, degradation, and mineralization for ARG, reduce the energy consumption significantly, and increase the current efficiency, indicating the superiority of the 2.5D electrode in ARG removal from wastewater. Through the experiments of temperature, concentration, and current density, it was found that the removal efficiency of ARG is more favorable at higher current density, average temperature, and lower concentration. Toxicity experiments revealed that, compared with the 2D electrode, the 2.5D electrode could significantly reduce the toxicity of wastewater, indicating the potential for reducing the toxicity of the dyeing wastewater.

Conflicts of Interest: The authors declare no conflict of interest.

References

1. Sarkka, H.; Bhatnagar, A.; Sillanpaa, M. Recent developments of electro-oxidation in water treatment—A review. *J. Electroanal. Chem.* **2015**, *754*, 46–56. [CrossRef]
2. Hao, X.; Hua, G.; Jiangtao, F.; Dan, W.; Zhengwei, L.; Yu, W.; Wei, Y. Electrochemical Oxidation Combined with Adsorption: A Novel Route for Low Concentration Organic Wastewater Treatment. *Int. J. Electrochem. Sci.* **2019**. [CrossRef]
3. Chaplin, B.P. Critical review of electrochemical advanced oxidation processes for water treatment applications. *Environ. Sci.-Proc. Impacts* **2014**, *16*, 1182–1203. [CrossRef] [PubMed]
4. Zhang, M.; Shi, Q.; Song, X.; Wang, H.; Bian, Z. Recent electrochemical methods in electrochemical degradation of halogenated organics: A review. *Environ. Sci. Pollut. Res. Int.* **2019**, *26*, 10457–10486. [CrossRef] [PubMed]
5. Radjenovic, J.; Sedlak, D.L. Challenges and Opportunities for Electrochemical Processes as Next-Generation Technologies for the Treatment of Contaminated Water. *Environ. Sci. Technol.* **2015**, *49*, 11292–11302. [CrossRef]
6. Jia, W.; Kai, Z.; Hao, X.; Wei, Y. Electrochemical oxidation of rhodamine B by PbO_2/Sb-SnO_2/TiO_2 nanotube arrays electrode. *Chin. J. Catal.* **2019**, *40*, 917–927.
7. Xiaoliang, L.; Hao, X.; Wei, Y. Fabrication and characterization of a PbO_2-TiN composite electrode by co-deposition method. *J. Electrochem. Soc.* **2016**, *163*, 592–602. [CrossRef]
8. Wu, W.; Huang, Z.-H.; Lim, T.-T. Recent development of mixed metal oxide anodes for electrochemical oxidation of organic pollutants in water. *Appl. Catal. A Gen.* **2014**, *480*, 58–78. [CrossRef]
9. Yao, Y.; Ren, B.; Yang, Y.; Huang, C.; Li, M. Preparation and electrochemical treatment application of Ce-PbO_2/ZrO_2 composite electrode in the degradation of acridine orange by electrochemical advanced oxidation process. *J. Hazard. Mater.* **2019**, *361*, 141–151. [CrossRef]
10. Liu, S.; Cui, T.; Xu, A.; Han, W.; Li, J.; Sun, X.; Shen, J.; Wang, L. Electrochemical treatment of flutriafol wastewater using a novel 3D macroporous PbO_2 filter: Operating parameters, mechanism and toxicity assessment. *J. Hazard. Mater.* **2018**, *358*, 187–197. [CrossRef]

11. Zhou, X.; Liu, S.; Yu, H.; Xu, A.; Li, J.; Sun, X.; Shen, J.; Han, W.; Wang, L. Electrochemical oxidation of pyrrole, pyrazole and tetrazole using a TiO_2 nanotubes based SnO_2-Sb/3D highly ordered macro-porous PbO_2 electrode. *J. Electroanal. Chem.* **2018**, *826*, 181–190. [CrossRef]

12. Duan, P.; Hu, X.; Ji, Z.; Yang, X.; Sun, Z. Enhanced oxidation potential of Ti/SnO_2-Cu electrode for electrochemical degradation of low-concentration ceftazidime in aqueous solution: Performance and degradation pathway. *Chemosphere* **2018**, *212*, 594–603. [CrossRef] [PubMed]

13. Zaviska, F.; Drogui, P.; Blais, J.F.; Mercier, G.; d'Auzay, S.D. Electrochemical Oxidation of Chlortetracycline Using Ti/IrO_2 and Ti/PbO_2 Anode Electrodes: Application of Experimental Design Methodology. *J. Environ. Eng.* **2013**, *139*, 810–821. [CrossRef]

14. Kaur, R.; Kushwaha, J.P.; Singh, N. Amoxicillin electro-catalytic oxidation using Ti/RuO_2 anode: Mechanism, oxidation products and degradation pathway. *Electrochim. Acta* **2019**, *296*, 856–866. [CrossRef]

15. Alcocer, S.; Picos, A.; Uribe, A.R.; Perez, T.; Peralta-Hernandez, J.M. Comparative study for degradation of industrial dyes by electrochemical advanced oxidation processes with BDD anode in a laboratory stirred tank reactor. *Chemosphere* **2018**, *205*, 682–689. [CrossRef]

16. Siedlecka, E.M.; Ofiarska, A.; Borzyszkowska, A.F.; Bialk-Bielinska, A.; Stepnowski, P.; Pieczynska, A. Cytostatic drug removal using electrochemical oxidation with BDD electrode: Degradation pathway and toxicity. *Water Res.* **2018**, *144*, 235–245. [CrossRef]

17. He, Y.; Wang, X.; Huang, W.; Chen, R.; Zhang, W.; Li, H.; Lin, H. Hydrophobic networked PbO_2 electrode for electrochemical oxidation of paracetamol drug and degradation mechanism kinetics. *Chemosphere* **2018**, *193*, 89–99. [CrossRef]

18. Comninellis, C.; Vercesi, G.P. Characterization of DSA-type oxygen evolving electrodes Choice of a coating. *J. Appl. Electrochem.* **1991**, *21*, 335–345. [CrossRef]

19. Xiaoliang, L.; Hao, X.; Wei, Y. Electrochemical oxidation of aniline by a novel Ti-TixHy-Sb-SnO_2 electrode. *Chin. J. Catal.* **2016**, *37*, 1860–1870.

20. Wachter, N.; Aquino, J.M.; Denadai, M.; Barreiro, J.C.; Silva, A.J.; Cass, Q.B.; Rocha-Filho, R.C.; Bocchi, N. Optimization of the electrochemical degradation process of the antibiotic ciprofloxacin using a double-sided beta-PbO2 anode in a flow reactor: Kinetics, identification of oxidation intermediates and toxicity evaluation. *Environ. Sci. Pollut. Res. Int.* **2019**, *26*, 4438–4449. [CrossRef]

21. Pieczyńska, A.; Ossowski, T.; Bogdanowicz, R.; Siedlecka, E. Electrochemical degradation of textile dyes in a flow reactor: Effect of operating conditions and dyes chemical structure. *Int. J. Environ. Sci. Technol.* **2018**, *16*, 929–942. [CrossRef]

22. Pacheco-Álvarez, M.O.A.; Picos, A.; Pérez-Segura, T.; Peralta-Hernández, J.M. Proposal for highly efficient electrochemical discoloration and degradation of azo dyes with parallel arrangement electrodes. *J. Electroanal. Chem.* **2019**, *838*, 195–203. [CrossRef]

23. Sun, W.; Sun, Y.; Shah, K.J.; Chiang, P.C.; Zheng, H. Electrocatalytic oxidation of tetracycline by Bi-Sn-Sb/gamma-Al_2O_3 three-dimensional particle electrode. *J. Hazard. Mater.* **2019**, *370*, 24–32. [CrossRef] [PubMed]

24. Mengelizadeh, N.; Pourzamani, H.; Saloot, M.K.; Hajizadeh, Y.; Parseh, I.; Parastar, S.; Niknam, N. Electrochemical Degradation of Reactive Black 5 Using Three-Dimensional Electrochemical System Based on Multiwalled Carbon Nanotubes. *J. Environ. Eng.* **2019**, *145*. [CrossRef]

25. Alighardashi, A.; Aghta, R.S.; Ebrahimzadeh, H. Improvement of Carbamazepine Degradation by a Three-Dimensional Electrochemical (3-EC) Process. *Int. J. Environ. Res.* **2018**, *12*, 451–458. [CrossRef]

26. Hao, X.; Wei, Y.; Honghui, Y. Surface Analysis of Ti/Sb-SnO_2/PbO_2 Electrode after Long Time Electrolysis. *Rare Met. Mater. Eng.* **2015**, *44*, 2637–2641. [CrossRef]

27. Shao, D.; Yan, W.; Li, X.; Xu, H. Fe_3O_4/Sb–SnO_2 Granules Loaded on Ti/Sb–SnO_2 Electrode Shell by Magnetic Force: Good Recyclability and High Electro-oxidation Performance. *ACS Sustain. Chem. Eng.* **2015**, *3*, 1777–1785. [CrossRef]

28. Shao, D.; Zhang, X.; Lyu, W.; Zhang, Y.; Tan, G.; Xu, H.; Yan, W. Magnetic Assembled Anode Combining PbO_2 and Sb-SnO_2 Organically as An Effective and Sustainable Electrocatalyst for Wastewater Treatment with Adjustable Attribution and Construction. *ACS Appl. Mater. Interfaces* **2018**, *10*, 44385–44395. [CrossRef]

29. Yao, Y.; Li, M.; Yang, Y.; Cui, L.; Guo, L. Electrochemical degradation of insecticide hexazinone with Bi-doped PbO_2 electrode: Influencing factors, intermediates and degradation mechanism. *Chemosphere* **2019**, *216*, 812–822. [CrossRef]

30. Li, X.; Shao, D.; Xu, H.; Lv, W.; Yan, W. Fabrication of a stable Ti/TiOxHy/Sb−SnO$_2$ anode for aniline degradation in different electrolytes. *Chem. Eng. J.* **2016**, *285*, 1–10. [CrossRef]

31. Shao, D.; Yan, W.; Li, X.L.; Yang, H.H.; Xu, H. A Highly Stable Ti/TiHx/Sb-SnO$_2$ Anode: Preparation, Characterization and Application. *Ind. Eng. Chem. Res.* **2014**, *53*, 3898–3907. [CrossRef]

32. Hao, X.; Wuqi, G.; Jia, W.; Jiangtao, F.; Honghui, Y.; Wei, Y. Preparation and characterization of titanium-based PbO$_2$ electrodes modified by ethylene glycol. *Rsc Adv.* **2016**, *6*, 7610–7617. [CrossRef]

33. Xu, H.; Yuan, Q.S.; Shao, D.; Yang, H.H.; Liang, J.D.; Feng, J.T.; Yan, W. Fabrication and characterization of PbO$_2$ electrode modified with [Fe(CN)(6)](3-) and its application on electrochemical degradation of alkali lignin. *J. Hazard. Mater.* **2015**, *286*, 509–516. [CrossRef]

34. Wilk, J.; Grosicki, S. Experimental study of electrochemical mass transfer in an annular duct with the electrolyte nanofluid. *Int. J. Therm. Sci.* **2018**, *129*, 280–289. [CrossRef]

35. Wilk, J. A review of measurements of the mass transfer in minichannels using the limiting current technique. *Exp. Therm. Fluid Sci.* **2014**, *57*, 242–249. [CrossRef]

36. Dalle, A.A.; Domergue, L.; Fourcade, F.; Assadi, A.A.; Djelal, H.; Lendormi, T.; Soutrel, I.; Taha, S.; Amrane, A. Efficiency of DMSO as hydroxyl radical probe in an Electrochemical Advanced Oxidation Process—Reactive oxygen species monitoring and impact of the current density. *Electrochim. Acta* **2017**, *246*, 1–8. [CrossRef]

37. Tai, C.; Peng, J.-F.; Liu, J.-F.; Jiang, G.-B.; Zou, H. Determination of hydroxyl radicals in advanced oxidation processes with dimethyl sulfoxide trapping and liquid chromatography. *Anal. Chim. Acta* **2004**, *527*, 73–80. [CrossRef]

38. Yingwu, Y.; Ganggang, T.; Yang, Y.; Chunjiao, H.; Baicheng, L.; Lin, G. Electrochemical oxidation of acetamiprid using Yb-doped PbO$_2$ electrodes: Electrode characterization, influencing factors and degradation pathways. *Sep. Purif. Technol.* **2019**, *211*, 456–466. [CrossRef]